CrossMark

ORIGINAL

Effects of rib size and arrangement on forced convective heat transfer in a solar air heater channel

Sompol Skullong · Chinaruk Thianpong ·
Pongjet Promvonge

Abstract The article presents an experimental investigation on turbulent heat transfer and friction loss behaviors of airflow through a constant heat-fluxed solar air heater channel fitted with rib turbulators. The experiment was conducted for the airflow rate in terms of Reynolds numbers based on the hydraulic diameter of the channel in a range of 5000–24,000. In the present work, a comparative study between square and thin ribs (90°-rib) with three rib arrangements, namely, one ribbed wall (or single rib), in-line and staggered ribs on two opposite walls was first introduced. The study shows a significant effect of the presence of the ribs on the heat transfer rate and friction loss over the smooth wall channel. The comparison made at a single rib pitch and height also revealed that the thin rib performs better than the corresponding square one. Among the three arrangements, the in-line rib array provides higher heat transfer and friction loss than the staggered and the single one. However, the staggered thin rib provides the highest thermal performance. With this reason, only the staggered thin ribs at four different relative heights ($B_R = 0.1$, 0.2, 0.3 and 0.4) and three relative pitches ($P_R = 0.5$, 0.75 and 1.33) are investigated further. It is found that the staggered rib at $B_R = 0.4$ and $P_R = 0.5$ yields the highest heat transfer and friction factor but the maximum thermal performance is at $B_R = 0.2$ and $P_R = 0.75$.

S. Skullong (✉)
Department of Mechanical Engineering, Faculty of Engineering
at Si Racha, Kasetsart University Sriracha Campus, 199 M.6,
Sukhumvit Rd., Sriracha, Chonburi 20230, Thailand
e-mail: sfengsps@src.ku.ac.th

C. Thianpong · P. Promvonge
Department of Mechanical Engineering, Faculty of Engineering,
King Mongkut's Institute of Technology Ladkrabang,
Bangkok 10520, Thailand

List of symbols

A	Heat transfer surface area (m²)
AR	Aspect ratio of channel ($=W/H$)
B_R	Rib blockage ratio ($=e/H$)
$C_{p,air}$	Specific heat capacity of air (J/kg K)
D_h	Hydraulic diameter ($=4WH/p$, m)
e	Rib height (m)
f	Friction factor
H	Channel height (m)
h	Average heat transfer coefficient (W/m² K)
I	Current (Å)
k	Thermal conductivity of air (W/m K)
L	Length of test channel (m)
$\dot{m}$	Air mass flow rate (kg/s)
Nu	Nusselt number ($=hD/k$)
P	Pitch (axial length of cycle, m)
p	Channel perimeter ($=2W + 2H$)
ΔP	Pressure drop (Pa)
P_R	Rib pitch to channel height ratio
Pr	Prandtl number
Re	Reynolds number ($=UD/\nu$)
Q	Heat transfer (W)
T	Temperature (K)
TEF	Thermal enhancement factor
t_b	Thickness of thin rib (m)
t_t	Thickness of square rib (m)
U	Mean velocity (m/s)
V	Voltage (V)
$\dot{V}$	Volumetric flow rate (m³/s)
W	Channel width (m)

Greek symbols

α	Angle of attack of rib (°)
ρ	Density of air (kg/m³)
ν	Kinematics viscosity (m²/s)

Subscripts

b   Bulk
0   Smooth channel
conv   Convection
i   Inlet
o   Out
pp   Pumping power
s   Channel surface

1 Introduction

The use of ribs/baffles placing in the cooling/heating channels or solar air heater channel heat exchangers is one of the commonly used passive heat transfer enhancement technique in single-phase internal flows. Hence, the research work on fluid flow and heat transfer in ribbed channels has been abundant so far. This heat transfer enhancement technique has been applied to various types of industrial applications such as shell-and-tube type heat exchangers, thermal power plants, chemical processing plants, air conditioning equipment, refrigerators, radiator for automobiles. Periodically positioned ribs/baffles in the channels interrupt hydrodynamic and thermal boundary layers. Downstream of each rib/baffle the flow separates, re-circulates and impinges on the channel wall and these effects are the main reasons for heat transfer enhancement in such channels. The use of ribs/baffles increases not only the heat transfer rate but also substantial the pressure loss. The rib/baffle geometry and arrangement in the channel also alter the flow field resulting in different the convective heat transfer coefficient and the overall thermal performance. There have been many types of rib/baffle tabulators [1–9] and the winglet vortex generators [10–12] employed in the heat exchanger channels.

In general, the swirl/vortex flow generator is used in augmentative heat transfer in several engineering applications to enhance the rate of the heat/mass transfer equipment such as heat exchanger [13], drying process, vortex combustor, refrigeration, gas turbine, etc. Several investigations have been conducted to study the effect of rib parameters on heat transfer and friction factor for two opposite roughened surfaces in channels. The performance of square, triangular and semi-circular ribs was experimentally investigated by Liou and Hwang [14] sing a real time laser holographic in terferometry to measure the local as well as average heat transfer coefficients. They found that the square ribs give the best heat transfer performance among them. This is contrary to the experimental result of Ahn [15] indicated that the triangular rib performs better than the square one. Murata and Mochizuki [16] studied numerically the heat transfer distribution in a ribbed square channel with e/D = 0.1, P/e = 10 and 60°
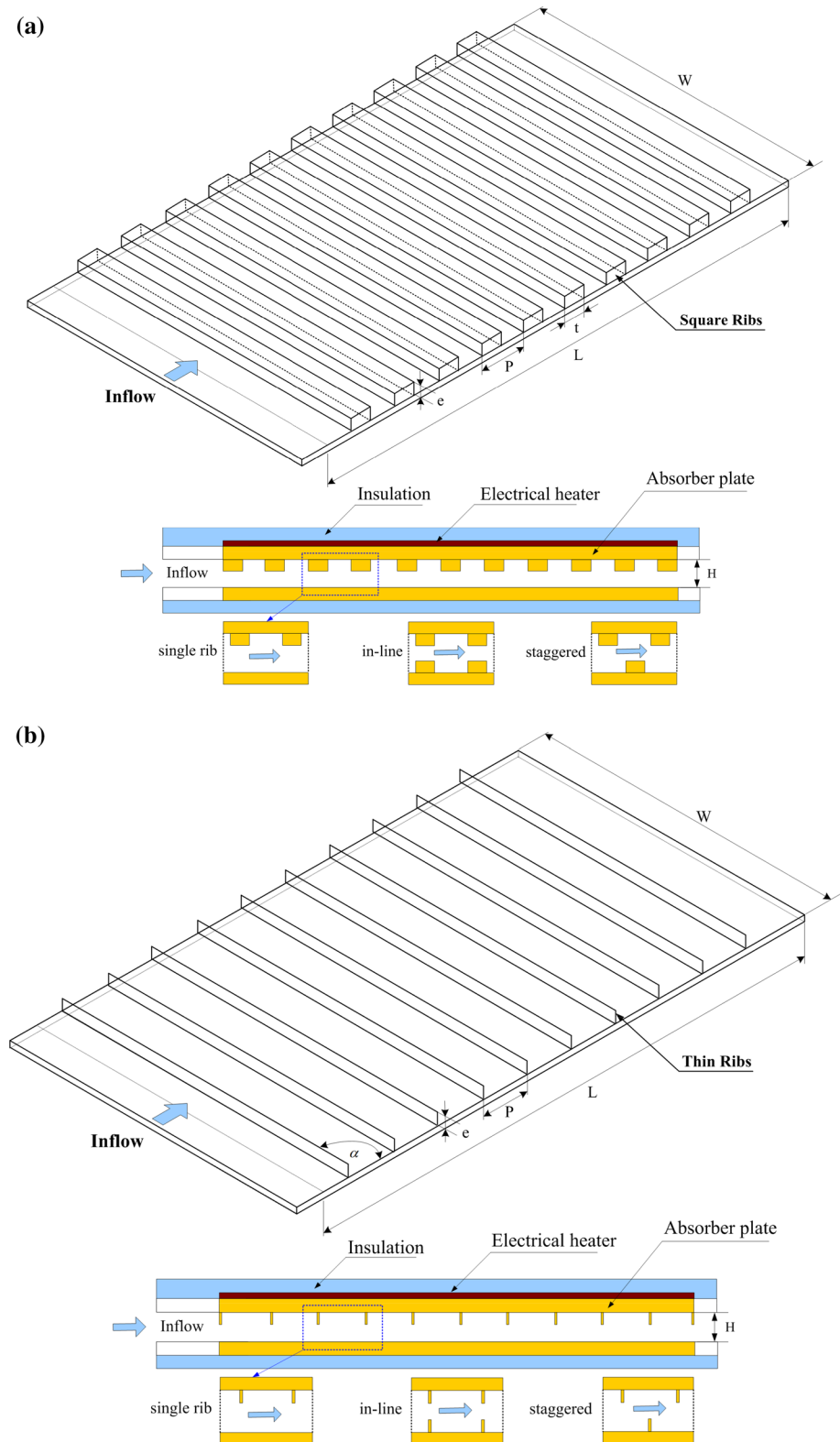
orientation using large eddy simulation. Their numerical result provided that the flow reattachment at the midpoint between ribs caused a significant increase in the local heat transfer. Taslim et al. [17] conducted a measurement of the heat transfer in a square channel with three blockage ratios (B_R = e/H = 0.083, 0.125 and 0.167) and a fixed P/e = 10 using a liquid crystal technique. Various staggered rib configurations were studied, especially for the angle of 45° and experimental data showed a significant increase in average Nusselt number with increasing the B_R value.

In addition, the use of ribs completely makes the change of the flow field and thus the distribution of the local heat transfer coefficient. Periodically mounted ribs in the absorber plate of solar air heater channels can help to interrupt hydrodynamic and thermal boundary layers leading to an increase in heat transfer rate. Several studies have been carried out to investigate the effect of rib geometry and arrangements on heat transfer and friction loss for roughened surfaces of heat exchanger channels or solar air heaters. Sahu and Bhagoria [18] examined broken transverse ribs in solar air heaters, reported that the roughened absorber plate yields the heat transfer rate at 1.25–1.4 times over the smooth rectangular duct and the maximum thermal efficiency is in the range of 51–83.5 %. Mittal et al. [19] studied and compared the absorber plate with six different types of roughness elements. Their results showed that the channel with inclined ribs including V-shaped ribs performs better heat transfer rate than others. An experiment of Aharwal et al. [20] was conducted to study heat transfer behaviors of a solar air heater channel with inclined square split-rib with a gap on one wall and the results showed that the gap in the inclined rib enhances the heat transfer of the channel. The increase in Nu and f was, respectively, in a range of 1.5–2.6 times and 2.3–2.9 times the smooth channel. Tamna et al. [21] studied experimentally and numerically on heat transfer and fluid flow in a solar air heater channel fitted with V-baffle vortex generators (BVGs). They found that at smaller pitch ratio (P_R), the in-line array provides the highest heat transfer and friction factor in comparison with the staggered and the single BVG. Prasad et al. [22] studied the effect of three sided artificially roughened solar air heater. Yadav and Bhagoria [23] numerically investigated the fluid flow and heat transfer characteristics of fully developed turbulent flow in a solar air heater duct with repeated transverse square ribs on the absorber plate and the rib with P/e = 10.71 and e/D = 0.042 yielded the best thermo-hydraulic performance parameter. The thermal performance of double pass solar air heaters were reported in Refs. [24, 25].

Chandra et al. [26] carried out measurements on heat transfer and pressure loss in a square channel with continuous ribs on one, two, three and four walls. They found that the heat transfer augmentation increases with the rise in the

number of ribbed walls. The effect of transverse, angled ribs, discrete, angled discrete ribs, V-shaped, V-shaped broken and parallel broken ribs on heat transfer and friction was studied by Tanda [27]. It was found that 90° transverse ribs provided the lowest thermal performance while the 60° parallel broken ribs or 60° V-shaped broken ribs yielded a higher heat transfer augmentation than the 45° parallel broken ribs or 45° V-shaped broken ribs. Parallel angled discrete ribs were seen to be superior to parallel angled full ribs and its 60° discrete ribs performed the highest heat transfer. Chang et al. [28] investigated heat transfer augmentation in a channel with deep dimples and scale-roughened walls while theoretical and numerical work on ribs was also reported by Katoh et al. [29]. Promvonge et al. [30] investigated numerically the turbulent periodic flows in a square duct with inline 60° V-shaped discrete thin ribs placed on two opposite walls. Extensive literature reviews over hundred references on various rib turbulators were reported by Hans et al. [31] and Saxena et al. [32]. Promvonge et al. [33, 34] studied experimentally and numerically the turbulent flow over 30° angle–finned tapes inserted diagonally in a square duct and pointed out that the smaller fin pitch spacing provided the highest heat transfer and friction factor. The thermal performance of the finned-tape turbulator was found to be much higher than that of the wire–coil/twisted–tape turbulator alone.

In the literature review above, most studies are mainly focused on square or low aspect ratio channels, rib height and pitch spacing ratios, and rib geometries. In solar air heater systems, the investigation on rib arrangements and sizes has rarely been reported, especially for thin ribs. This is very fruitful for improvement of solar thermal systems. Therefore, the main aim of the present work is to extend the experimental data available on various sizes of transverse ribs with three rib arrangements, namely, one ribbed wall, in-line and staggered arrays. In addition, the staggered thin ribs with different B_R and P_R values are further investigated and the optimal staggered rib is also suggested. Experimental results using air as the test fluid are presented in turbulent channel flows for Reynolds number (Re) from 5000 to 24,000.

2 Experimental setup

The experiments were conducted to examine the effect of using square ribs and thin ribs on heat transfer and flow friction characteristics of airflow in a rectangular solar air heater channel. A schematic diagram of the experimental setup is illustrated in Fig. 1 and the details of 90° square ribs and thin ribs placed on one wall and two opposite walls with in-line and staggered arrays are depicted in Fig. 2a, b, respectively. In the experimental setup, a circular pipe was used for connecting a high-pressure blower to a settling tank, which an orifice flow-meter was mounted in this pipeline while a channel including a calm section and a test section was employed following the settling tank.

The channel configuration was characterized by the channel height (H) of 30 mm and the width (W) of 300 mm. The overall length of the channel was 2000 mm which included length of the test section (L) of 440 mm. The form of the square-ribbed plate was accomplished by means of wire-EDM machining. The test channel was mounted repeatedly with square ($t_t = 6$ mm) and thin ($t_b = 0.5$ mm) ribs having a single axial pitch, $P = 40$ mm (relative pitch,

Fig. 1 Schematic diagram of experimental apparatus

Fig. 2 Test section with transverse **a** square and **b** thin ribs

P$_R$ = 1.33) and a rib height, $e = 6$ mm (B$_R$ = 0.2). Furthermore, the staggered thin ribs with four different relative heights (B$_R$ = e/H = 0.1, 0.2, 0.3 and 0.4) and three relative pitches (P$_R$ = P/H = 0.5, 0.75 and 1.33) were also offered and a constant heat-flux was applied on the upper wall only (absorber plate).

The AC power supply was the source of power for the plate-type heater, used for heating the upper-plate of the

test section only to maintain uniform surface heat flux. Air as the tested fluid, was directed into the systems by a 1.45 kW high-pressure blower. The operating speed of the blower was varied by using an inverter to provide desired air flow rates. The flow rate of air in the systems was measured by an orifice plate. The pressure across the orifice was measured using inclined manometer. In order to measure temperature distributions on the principal upper wall, twelve thermocouples were fitted to the wall. The thermocouples were installed in holes drilled from the rear face and centered of the walls with the respective junctions positioned within 2 mm of the inside wall and axial separation was 40 mm apart. To measure the inlet and outlet temperatures, two RTD (Pt100) thermocouples were positioned upstream and downstream of the test channel. The thermocouple voltage outputs were fed into a data acquisition system (Fluke 2650A) and then recorded via a personal computer. Two static pressure taps were located at the top of the principal channel to measure axial pressure drops across the test section, used to evaluate average friction factor. These were located at the centre line of the channel. One of these taps is 120 mm downstream from the leading edge of the channel and the other is 50 mm upstream from the trailing edge. The pressure drop was measured by a digital differential pressure and a data logger connected to the 2 mm diameter taps and recorded via a personal computer.

The uncertainty in the data calculation was based on Ref. [35]. The maximum uncertainties of non-dimensional parameters were ±5 % for Reynolds number, ±6 % for Nusselt number and ±8 % for friction factor.

3 Data processing

The aim of this work is to investigate the Nusselt number (Nu) in transverse-ribbed channels. The independent parameters are Re and rib arrangements. The Re based on the channel hydraulic diameter is given by

$$Re = UD_h/\nu \tag{1}$$

The local heat transfer coefficients are evaluated from the measured temperatures and heat inputs. The average heat transfer coefficient due to heat added uniformly to fluid (Q_{air}) and the temperature difference of surface and fluid ($T_s - T_b$), will be calculated from the experimental data via the following equations:

$$Q_{air} = Q_{conv} = \dot{m}C_p(T_o - T_i) = VI - heatlosses \tag{2}$$

$$Q_{conv} = W \int h_x (T_s - T_{bx})\, dx$$
$$= W\overline{(T_{sx} - T_{bx})}hL = \left(\tilde{T}_s - T_b\right)Ah$$

As found, the heat absorbed by the fluid for thermal equilibrium test is within 4 % lower than the heat supplied by electrical winding in the test channel due to convection heat losses from the test section to surroundings. For data analysis, only the heat transfer rate absorbed by the air is taken for internal convective heat transfer coefficient calculation. Thus, the average heat transfer coefficient can be written as follows:

$$h = \frac{\dot{m}C_p(T_o - T_i)}{A\left(\tilde{T}_s - T_b\right)} \tag{3}$$

in which,

$$T_b = (T_o + T_i)/2 \tag{4}$$

and

$$\tilde{T}_s = \sum T_s/12 \tag{5}$$

The term A is the convective heat transfer area of the upper channel wall whereas $\tilde{T}_s$ is the average surface temperature obtained from local surface temperatures along the axial length of the heated channel. Then, average Nu is written as:

$$Nu = \frac{hD_h}{k} \tag{6}$$

The friction factor (f) is evaluated by:

$$f = \frac{2}{(L/D_h)}\frac{\Delta P}{\rho U^2} \tag{7}$$

where ΔP is a pressure drop across the test section and U is mean air velocity of the channel. All of thermo-physical properties of the air are determined at the overall bulk air temperature from Eq. (4)

For a constant pumping power,

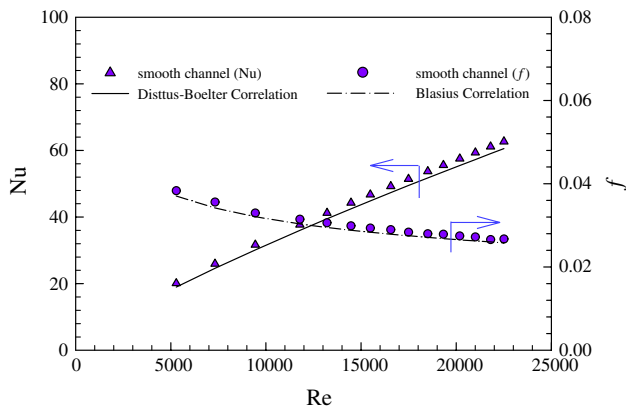$$\left(\dot{V}\Delta P\right)_0 = \left(\dot{V}\Delta P\right) \tag{8}$$

and the relationship between f and Re can be expressed as:

$$\left(f Re^3\right)_0 = \left(f Re^3\right)$$
$$Re_0 = Re\left(f/f_0\right)^{1/3} \tag{9}$$

The thermal enhancement factor (TEF), defined as the ratio of the heat transfer coefficient, h of an augmented surface to that of a smooth surface, h_0, at a constant pumping power:

$$TEF = \left.\frac{h}{h_0}\right|_{pp} = \left.\frac{Nu}{Nu_0}\right|_{pp} = \left(\frac{Nu}{Nu_0}\right)\left(\frac{f}{f_0}\right)^{-1/3} \tag{10}$$

Fig. 3 Verification of Nu and *f* for smooth channel

Correlation of Dittus-Boelter,

$$Nu = 0.023Re^{0.8}Pr^{0.4} \quad \text{for} \quad \text{heating}. \tag{11}$$

Correlation of Blasius,

$$f = 0.316Re^{-0.25} \tag{12}$$

Figure 3 show a comparison of Nu and *f* obtained from the present work with those from correlations of Eqs. (11) and (12). In the figure, the present results reasonably agree well within ±6 and ±7 % for the Nu and *f* correlations, respectively.

4 Results and discussion

The present work on both heat transfer and pressure loss behaviors in a ribbed channel with aspect ratio AR = 10 is presented.

4.1 Verification of smooth channel

The present experimental results on heat transfer and friction characteristics in a smooth wall channel are first validated in terms of Nusselt number (Nu) and friction factor (*f*). The Nu and *f* obtained from the present smooth channel are, respectively, compared with those from the correlations of Dittus-Boelter and Blasius found in the open literature [36] for turbulent flow in ducts.

4.2 Effect of rib size

The present experimental results on heat and flow friction characteristics in a uniform heat-flux solar air heater channel fitted with different thickness of transverse ribs attached repeatedly with the three rib arrangements over a range of Re as mentioned earlier.

4.2.1 Heat transfer

The Nu for all the cases investigated is presented in Fig. 4a. In the figure, both square and thin ribs yield considerable heat transfer enhancement with similar trends in comparison with the smooth channel. The Nu is found to increase with the increment of Re for both ribs. The thin rib provides higher heat transfer rate than the square one, at a similar operating condition. This is because the thin rib turbulators interrupt the development of thermal boundary layer of the fluid flow and increase the turbulence intensity of the flow. It is interesting to note that the heat transfer in the form of
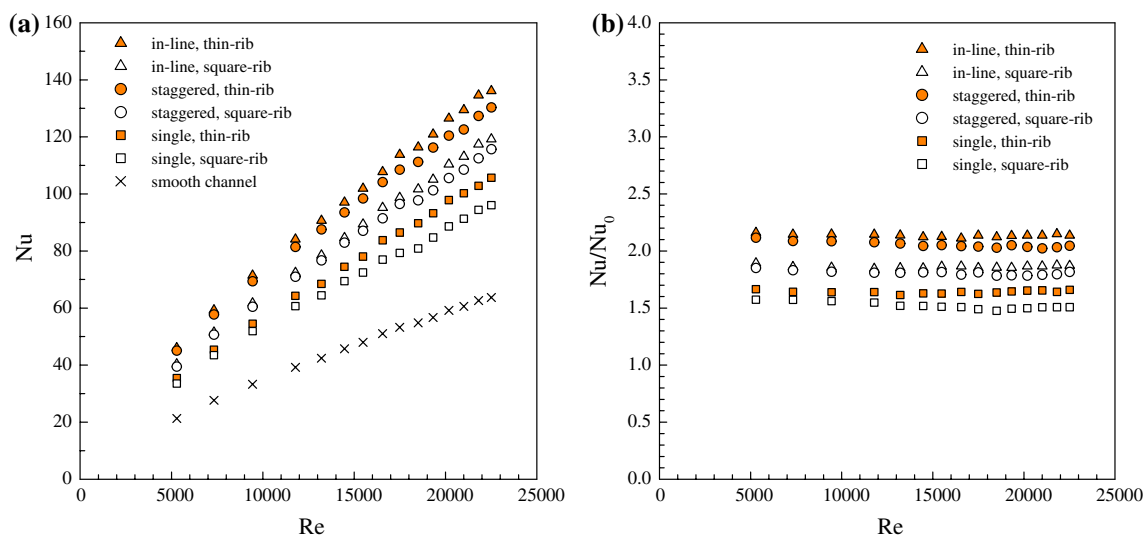
Fig. 4 Variation of **a** Nu and **b** Nu/Nu$_0$ with Re

Nu for the in-line thin rib is considerably higher than that for the staggered one which performs better than the single rib. This is because the in-line thin rib can strongly interrupt the flow and divert its direction, promoting high levels of mixing over the others. For the thin rib, the increases in Nu for using in-line, staggered and single rib are in a range of 213–216, 204–211 and 164–165 % over the smooth channel, respectively.

The Nusselt number ratio, Nu/Nu_0, defined as a ratio of augmented Nu to Nu of smooth channel plotted against the Re value is displayed in Fig. 4b. In the figure, the Nu/Nu_0 tends to be nearly uniform with the rise of Re for all rib arrangements. It is worth noting that the Nu/Nu_0 is highest for the in-line thin rib. The thin rib performs better than the square one. The average Nu/Nu_0 values for the ribs with in-line, staggered and single rib arrays are, respectively, around 2.13, 2.05 and 1.64 for the thin rib and about 1.86, 1.81 and 1.52 for the square one.

4.2.2 Friction factor

The effect of the 90°-ribs or transverse ribs on the isothermal pressure drop across the tested channel is depicted in Fig. 5a. The variation of the pressure drop is shown in terms of f with Re. In the figure, it is apparent that the use of the rib turbulators leads to a substantial increase in f over the smooth channel. This can be attributed to flow blockage, higher surface area and the act caused by the reverse flow due to the presence of the ribs. Also, the thin rib gives rise to higher pressure drop than the square one for all similar cases. As expected, the f from the thin rib with in-line array is substantially higher than that with staggered array while the one ribbed wall yields the lowest f. The mean

increase in f of the ribs is in a range of 3.1–7.1 times the smooth channel. The f value of the in-line thin rib is found to be about 17 % above the staggered one and about 36.5 % over the single rib.

Figure 5b presents the variation of the friction factor ratio, f/f_0, with Re values. It is visible that the f/f_0 tends to increase with the increment of Re, especially for the in-line thin rib. The in-line rib provides a considerable increase in the f/f_0 over the staggered and the single ribs under the same conditions. The f/f_0 values for the in-line, staggered and single ribs are, respectively, about 5.2–7, 4.4–5.7 and 3.3–4.4 for the thin ribs and about 4.1–5.5, 3.6–4.7 and 3.1–4.1 for the square ribs, depending on Re values. This suggests that the employ of staggered ribs can help reduce the pressure loss considerably.

4.2.3 Thermal performance

Figure 6 shows the variation of the thermal enhancement factor (TEF) with Re for all rib arrangements. The data all obtained by measured Nu and f values are compared at a similar pumping power. In general, the TEF tends to decrease with the rise of Re for all rib cases. It is worth noting that the TEF values of the staggered thin ribs are highest. The TEF of the staggered thin rib is found to be the best among all rib turbulators applied and is about 1.3 at the lowest Re while that of the in-line one is slightly lower. For thin ribs with single wall rib, in-line and staggered ribs, the maximum TEF values are, respectively, about 1.1, 1.25 and 1.3. It is seen that the staggered thin rib gives the highest TEF at lower Re. At a given rib, the use of thin rib yields the TEF around 3–7 % higher than that of the square one. Because of considerably higher Nu and TEF, only the
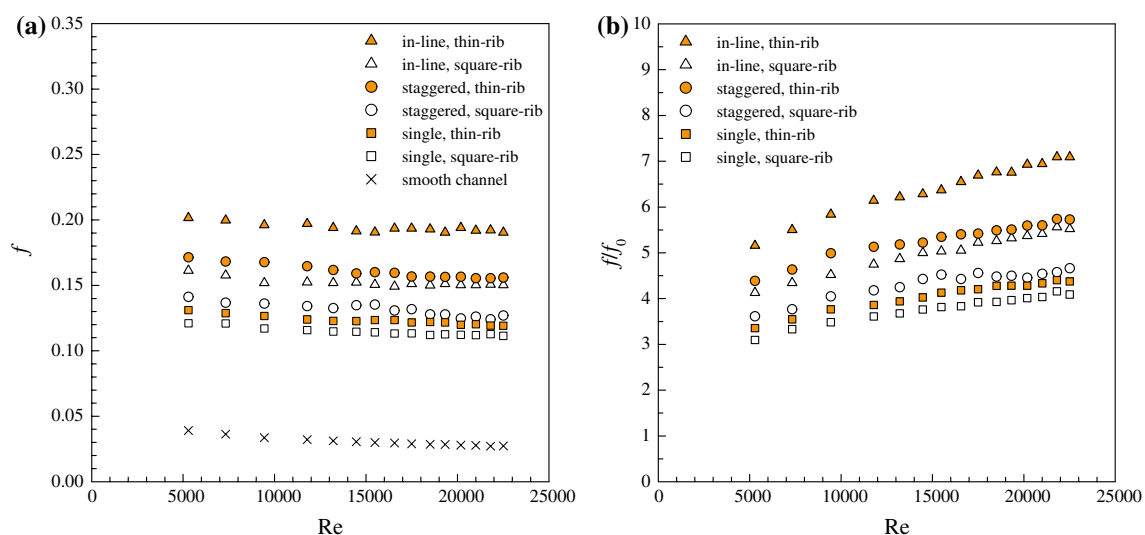
Fig. 5 Variation of **a** f and **b** f/f_0 with Re
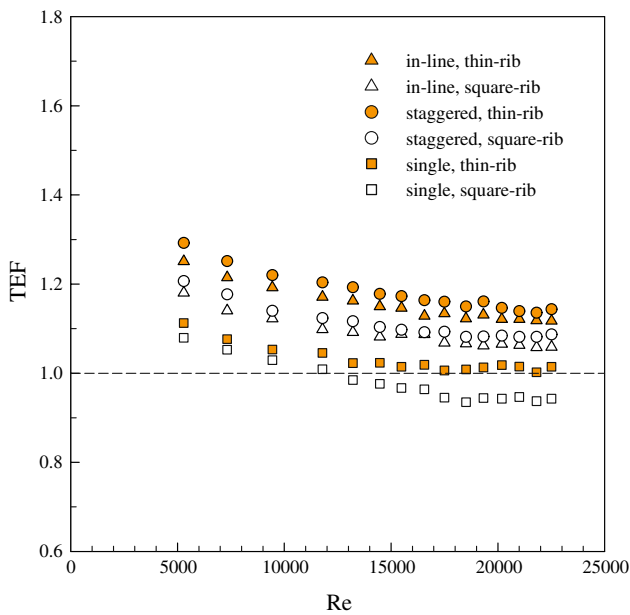
Fig. 6 Variation of TEF with Re

staggered thin ribs will be further investigated in the subsequent section.

4.3 Effect of staggered thin rib turbulators

4.3.1 Heat transfer

Figure 7a, b, respectively, present the Nu and Nu/Nu_0 in a solar air heater channel mounted periodically with staggered thin ribs at various B_R and P_R values. It is visible in Fig. 7a that the Nu for the staggered ribs increases with the rise of Re and of B_R values. The smaller P_R provides higher

heat transfer rate than the larger one at a given B_R. The heat transfer rates of the staggered ribs with $B_R = 0.4, 0.3, 0.2$ and 0.1, are, respectively, around 402, 383, 360 and 310 %; 370, 348, 316 and 276 %; and 265, 245, 205 and 177 % above the smooth channel for $P_R = 0.5, 0.75$ and 1.33. This is because the turbulence promoter by the staggered ribs with larger B_R is sufficiently strong to yield a mixing intensity of flow between the wall and the core regions while the larger P_R gives an opposite trend as can be seen in Fig. 7b. A close examination reveals that the Nu/Nu_0 of the staggered ribs is nearly independent of Re.

4.3.2 Friction factor

The variation of isothermal f and f/f_0 values with Re for staggered thin ribs at four B_R and three P_R values is depicted in Fig. 8a, b, respectively. In Fig. 8a, the f for the larger B_R is found to be considerably higher than that for the lower one and tends to be almost free from Re. The rise in f for the staggered ribs is much higher than that for the smooth channel, especially for the ribs at $B_R = 0.4$ and $P_R = 0.5$. The f for $P_R = 0.5$ is found to be considerably higher than that for $P_R = 0.75$ and 1.33. In Fig. 8b, the f/f_0 is found to increase with the increment of Re and B_R while it shows the reversing trend with increasing P_R. The mean increases in f/f_0 at $B_R = 0.4, 0.3, 0.2$ and 0.1 are, respectively, about 31.5, 25.8, 18.3 and 12.6; 22.1 17.4, 11.5 and 8.1; and 14.5 10.6, 5.3 and 3.7 times for $P_R = 0.5, 0.75$ and 1.33.
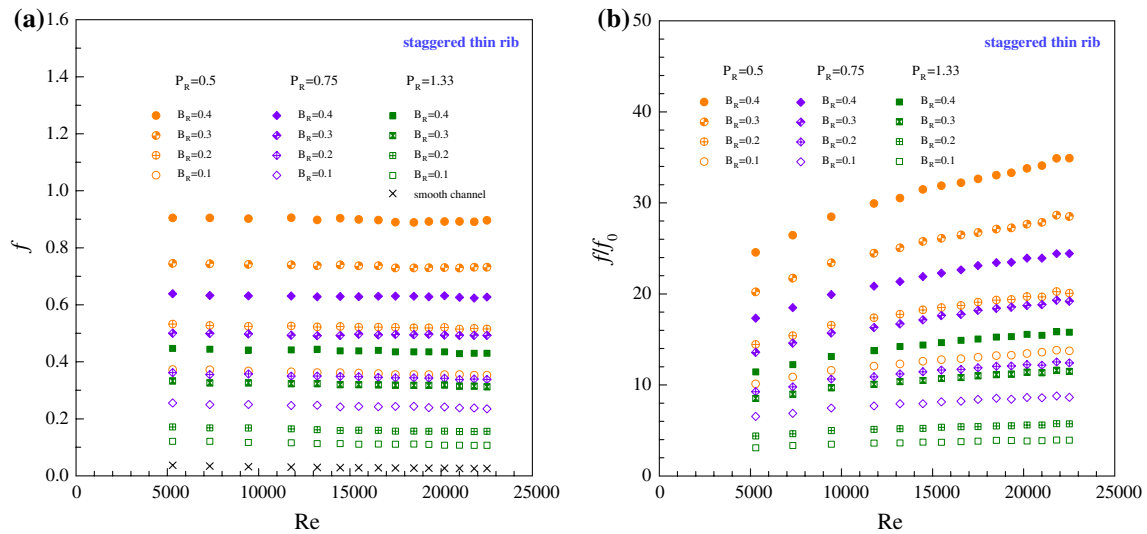
4.3.3 Thermal performance

Figure 9 displays the variation of TEF with Re and B_R for using the staggered thin rib under a similar pumping
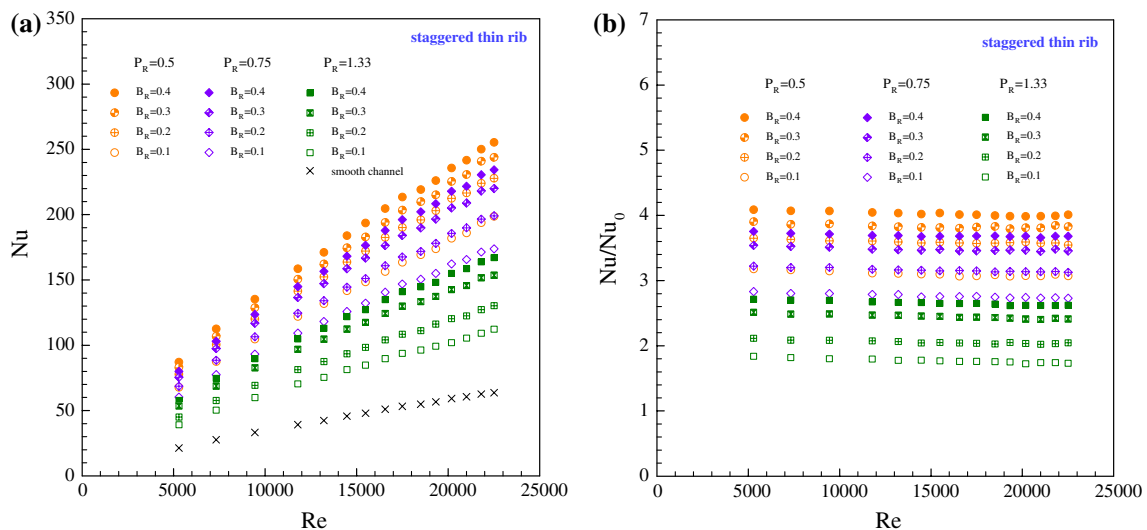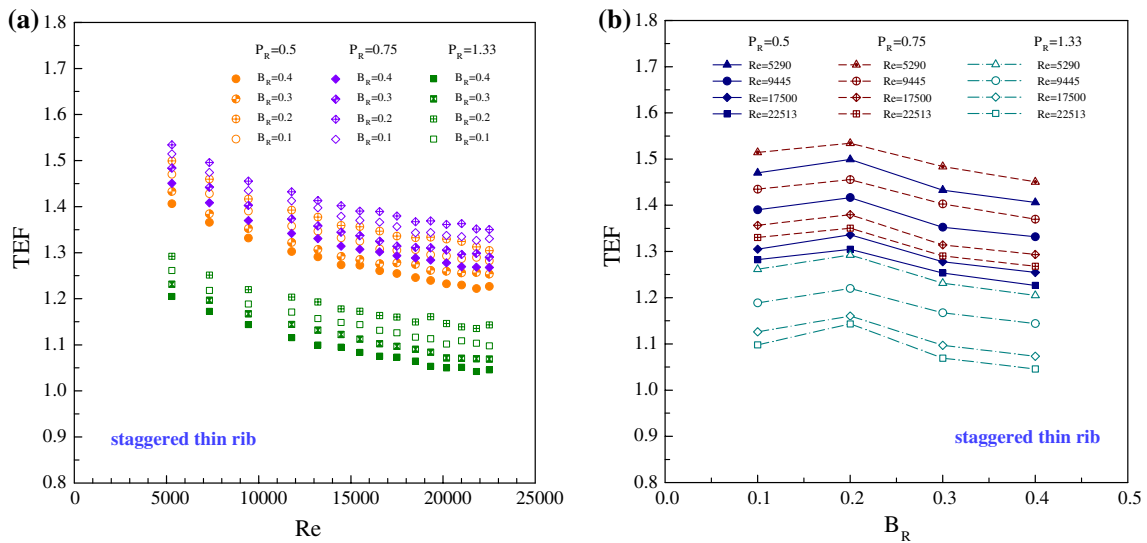

Fig. 7 Variation of **a** Nu and **b** Nu/Nu_0 with Re for staggered thin ribs

Fig. 8 Variation of **a** f and **b** f/f_0 with Re for staggered thin ribs

**Fig. 9** Variation of TEF **a** Re and **b** B_R for staggered thin ribs

power. In Fig. 9a, the TEF tends to decrease with the increase of Re. The rib at $B_R = 0.2$ and $P_R = 0.75$ gives the highest TEF around 1.53 at lower Re. The mean TEF values with $B_R = 0.4$, 0.3, 0.2 and 0.1 are, respectively, around 1.28, 1.3, 1.37 and 1.33; 1.32, 1.35, 1.4 and 1.38; and 1.1, 1.12, 1.18 and 1.15 for $P_R = 0.5$, 0.75 and 1.33. At a given B_R, the $P_R = 0.75$ yields the TEF around 3 and 16 % higher than the $P_R = 0.5$ and 1.33, respectively. The maximum TEF is found for the rib with $B_R = 0.2$ and $P_R = 0.75$ at the lowest Re, indicating the optimal point for the staggered-ribbed channel should be in this region as can be seen in Fig. 9b. The present TEF result is found to be much higher than the square rib as reported in

previous investigations [1, 6]. This is because it can generate reverse/recirculation flows along the test channel, leading to higher turbulence intensity and also heat transfer coefficient.

4.4 Empirical correlations

More details for the establishment of empirical correlations can be seen in Refs. [37–39]. In this research, the Nu and f values for the staggered thin ribs correlated with Re, Prandtl number (Pr), B_R and P_R, as formulated in Eqs. (13), (14), are plotted against measured data as depicted in Fig. 10a, b, respectively. Majority of the measured data
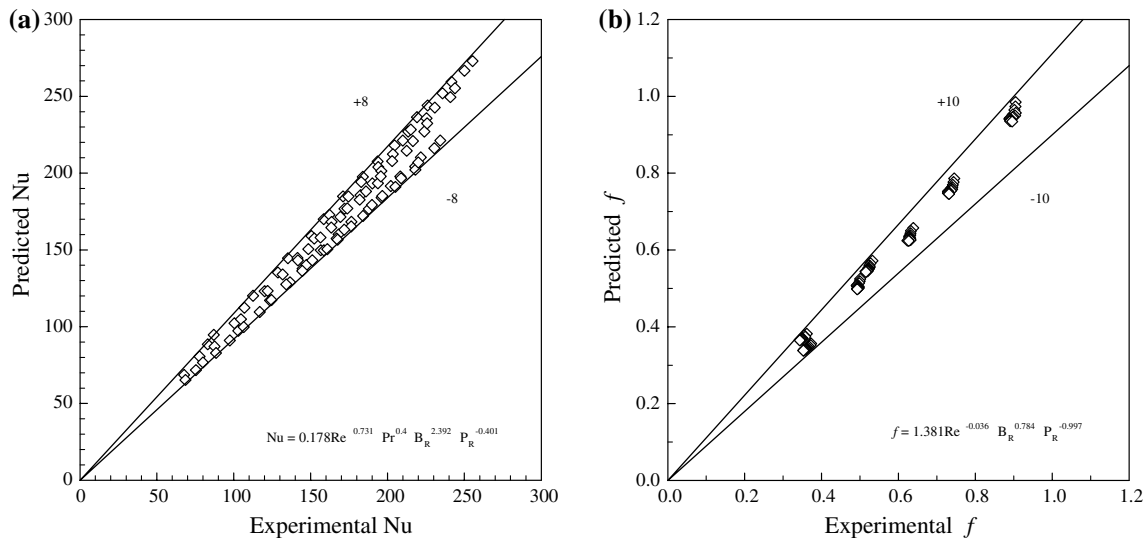
Fig. 10 Predicted data of **a** Nu and **b** f versus experimental data

falls within ± 8 and ± 10 % for the predicted Nu and f, respectively.

Correlations for Nu and f of the staggered thin ribs valid for $B_R = 0.4$, 0.3, 0.2 and 0.1; $P_R = 0.5$, 0.75 and 1.33; and Re = 5000–24,000 are developed as follows:

$$\mathrm{Nu} = 0.178\mathrm{Re}^{0.731}\mathrm{Pr}^{0.4}B_R^{2.392}P_R^{-0.401} \tag{13}$$

$$f = 1.381\mathrm{Re}^{-0.036}B_R^{0.784}P_R^{-0.997} \tag{14}$$

5 Conclusions

An experimental study has been carried out to investigate airflow friction and heat transfer characteristics in a solar air heater channel fitted with different rib geometry and with staggered thin ribs at different B_R and P_R for the turbulent regime, Re of 5000–24,000. The summary results can be drawn as follows:

- The use of rib turbulators with in-line array causes a very high pressure drop, especially for the thin rib and also provides considerable heat transfer augmentations, $\mathrm{Nu/Nu_0} = 2.13$–2.16.
- The thin rib provides higher heat transfer rate, friction factor and thermal enhancement factor than the square rib. Thus, the use of thin rib turbulator yields the TEF around 3–7 % higher than that of the square rib, especially for the staggered thin rib.
- The Nu of the staggered thin rib shows the uptrend with the rise in Re and B_R, but the downtrend with increasing P_R.
- In comparison, the staggered thin rib with $B_R = 0.2$ and $P_R = 0.75$ provides the highest TEF.

- The staggered square rib at $B_R = 0.2$ and $P_R = 1.33$ yields the highest TEF of about 1.21 while the staggered thin rib at $B_R = 0.2$ and $P_R = 0.75$ provides the highest TEF around 1.53 at lower Re, leading to more compact heat exchanger.

References

1. Thianpong C, Chompookham T, Skullong S, Promvonge P (2009) Thermal characterization of turbulent flow in a channel with isosceles triangular ribs. Int Commun Heat Mass Transfer 36:712–717
2. Sripattanapipat S, Promvonge P (2009) Numerical analysis of laminar heat transfer in a channel with diamond-shaped baffles. Int Commun Heat Mass Transfer 36:32–38
3. Promvonge P, Sripattanapipat S, Tamna S, Kwankaomeng S, Thianpong C (2010) Numerical investigation of laminar heat transfer in a square channel with 45° inclined baffles. Int Commun Heat Mass Transfer 37:170–177
4. Sriromreun P, Thianpong C, Promvonge P (2012) Experimental and numerical study on heat transfer enhancement in a channel with Z-shaped baffles. Int Commun Heat Mass Transfer 39:945–952
5. Skullong S, Kwankaomeng S, Thianpong C, Promvonge P (2014) Thermal performance of turbulent flow in a solar air heater channel with rib-groove turbulators. Int Commun Heat Mass Transfer 50:34–43
6. Promvonge P, Thianpong C (2008) Thermal performance assessment of turbulent channel flow over different shaped ribs. Int Commun Heat Mass Transfer 35:1327–1334
7. Gao X, Sunden B (2001) Heat transfer distribution in rectangular duct with V-shaped ribs. Heat Mass Transfer 37:315–320
8. Wang L, Sunden B (2007) Experimental investigation of local heat transfer in a square duct with various-shaped ribs. Heat Mass Transfer 43:759–766
9. Kumar A, Saini RP, Saini JS (2015) Effect of roughness width ratio in discrete multi v-shaped rib roughness on thermohydraulic performance of solar air heater. Heat Mass Transfer 51:209–220

10. Chompookham T, Thianpong C, Kwankaomeng S, Promvonge P (2010) Heat transfer augmentation in a wedge-ribbed channel using winglet vortex generators. Int Commun Heat Mass Transfer 37:163–169
11. Promvonge P, Khanoknaiyakarn C, Kwankaomeng S, Thianpong C (2011) Thermal behavior in solar air heater channel fitted with combined rib and delta-winglet. Int Commun Heat Mass Transfer 38:749–756
12. Skullong S, Promvonge P (2014) Experimental investigation on turbulent convection in solar air heater channel fitted with delta winglet vortex generator. Chin J Chem Eng 22:1–10
13. Chen YY, Song KW, Wang LB, Sun DL (2009) Comparisons of local experimental results with numerical results of heat transfer enhancement of a flat tube bank fin with vortex generators. Numer Heat Transfer Part A Appl 55:144–162
14. Liou TM, Hwang JJ (1993) Effect of ridge shapes on turbulent heat transfer and friction in a rectangular channel. Int J Heat Mass Transfer 36:931–940
15. Ahn SW (2001) The effects of roughness types on friction factors and heat transfer in roughened rectangular duct. Int Commun Heat Mass Transfer 28:933–942
16. Murata A, Mochizuki S (2001) Comparison between laminar and turbulent heat transfer in a stationary square duct with transverse or angled rib turbulators. Int J Heat Mass Transfer 44:1127–1141
17. Taslim ME, Li T, Kercher DM (1996) Experimental heat transfer and friction in channels roughened with angled, V-shaped, and discrete ribs on two opposite walls. ASME J Turbomach 118:20–28
18. Sahu MM, Bhagoria JL (2005) Augmentation of heat transfer coefficient by using 90° broken transverse ribs on absorber plate of solar air heater. Renew Energy 30:2057–2063
19. Mittal MK, Varun, Saini RP, Singal SK (2007) Effective efficiency of solar air heaters having different types of roughness elements on absorber plate. Energy 32:739–745
20. Aharwal KR, Gandhi BK, Saini JS (2008) Experimental investigation on heattransfer enhancement due to a gap in an inclined continuous rib arrangement in a rectangular duct of solar air heater. Renew Energy 33:585–596
21. Tamna S, Skullong S, Thianpong C, Promvonge P (2014) Heat transfer behaviors in a solar air heater channel with multiple V-baffle vortex generators. Sol Energy 110:720–735
22. Prasad BN, Behura Arun K, Prasad L (2014) Fluid flow and heat transfer analysis for heat transfer enhancement in three sided artificially roughened solar air heater. Sol Energy 105:27–35
23. Yadav AS, Bhagoria JL (2014) A numerical investigation of square sectioned transverse rib roughened solar air heater. Int J Therm Sci 79:111–131
24. Singh S, Dhiman P (2014) Thermal and thermohydraulic performance evaluation of a novel type double pass packed bed solar air heater under external recycle using an analytical and RSM (response surface methodology) combined approach. Energy 72:344–359
25. Dhiman P, Singh S (2015) Recyclic double pass packed bed solar air heaters. Int J Therm Sci 87:215–227
26. Chandra PR, Alexander CR, Han JC (2003) Heat transfer and friction behaviour in rectangular channels with varying number of ribbed walls. Int J Heat Mass Transfer 46:481–495
27. Tanda G (2004) Heat transfer in rectangular channels with transverse and V-shaped broken ribs. Int J Heat Mass Transfer 47:229–243
28. Chang SW, Liou TM, Lu MH (2005) Heat transfer of rectangular narrow channel with two opposite scale roughened walls. Int J Heat Mass Transfer 48:3921–3931
29. Katoh K, Choi K, Azuma T (2000) Heat-transfer enhancement and pressure loss by surface roughness in turbulent channel flows. Int J Heat Mass Transfer 43:4009–4017
30. Promvonge P, Changcharoen W, Kwankaomeng S, Thianpong C (2011) Numerical heat transfer study of turbulent square-duct flow through inline V-shaped discrete ribs. Int Commun Heat Mass Transfer 38:1392–1399
31. Hans VS, Saini RP, Saini JS (2009) Performance of artificially roughened solar air heaters—a review. Renew Sustain Energ Rev 13:1854–1869
32. Saxena A, Varun, El-Sebaii AA (2015) A thermodynamic review of solar air heaters. Renew Sust Energ Rev 43:863–890
33. Promvonge P, Skullong S, Kwankaomeng S, Thianpong C (2012) Heat transfer in square duct fitted diagonally with angle-finned tape—Part 1: experimental study. Int Commun Heat Mass Transfer 39:617–624
34. Promvonge P, Skullong S, Kwankaomeng S, Thianpong C (2012) Heat transfer in square duct fitted diagonally with angle-finned tape-Part 2: numerical study. Int Commun Heat Mass Transfer 39:625–633
35. ANSI/ASME, 1986. Measurement uncertainty. PTC 19, 1–1985. Part I
36. Incropera F, Dewitt PD (2007) Fundamentals of heat and mass transfer, 6th edn. Wiley, USA
37. Sethi M, Varun, Thakur NS (2012) Correlations for solar air heater duct with dimpled shape roughness elements on absorber plate. Sol Energy 86:2852–2861
38. Kumar A, Saini PR, Saini JS (2013) Development of correlations for Nusselt number and friction factor for solar air heater with roughened duct having multi v-shaped with gap rib as artificial roughness. Renew Energy 58:151–163
39. Aharwal KR, Pawar CB, Chaube A (2014) Heat transfer and fluid flow analysis of artificially roughened ducts having rib and groove roughness. Heat Mass Transfer 50:835–847